# Dosimetry of high-energy electron linac produced photoneutrons and the bremsstrahlung gamma-rays using TLD-500 and TLD-700 dosimeter pairs

Bhaskar Mukherjee[a,*], Dariusz Makowski[b], Stefan Simrock[a]

[a]*Deutsches Elektronen-Synchrotron (DESY), Notkestrasse 85, Hamburg D-22607, Germany*
[b]*Department of Microelectronics and Computer Science, Technical University of Lodz, Al. Politechniki 11, Lodz 93-590, Poland*

## Abstract

The neutron and gamma doses are crucial to interpreting the radiation effects in microelectronic devices operating in a high-energy accelerator environment. This report highlights a method for an accurate estimation of photoneutron and the accompanying bremsstrahlung (gamma) doses produced by a 450 MeV electron linear accelerator (linac) operating in pulsed mode. The principle is based on the analysis of thermoluminescence glow-curves of TLD-500 (Aluminium Oxide) and TLD-700 (Lithium Fluoride) dosimeter pairs. The gamma and fast neutron response of the TLD-500 and TLD-700 dosimeter pairs were calibrated with a $^{60}$Co (gamma) and a $^{241}$Am–Be ($\alpha$, n) neutron standard-source, respectively. The Kinetic Energy Released in Materials (kerma) conversion factor for photoneutrons was evaluated by folding the neutron kerma (dose) distribution in $^{7}$LiF (the main component of the TLD-700 dosimeter) with the energy spectra of the $^{241}$Am–Be ($\alpha$, n) neutrons and electron accelerator produced photoneutrons. The neutron kerma conversion factors for $^{241}$Am–Be neutrons and photoneutrons were calculated to be $2.52 \times 10^{-3}$ and $1.37 \times 10^{-3}$ μGy/a.u. respectively. The bremsstrahlung (gamma) dose conversion factor was evaluated to be $7.32 \times 10^{-4}$ μGy/a.u. The above method has been successfully utilised to assess the photoneutron and bremsstrahlung doses from a 450 MeV electron linac operating at DESY Research Centre in Hamburg, Germany.
© 2005 Elsevier B.V. All rights reserved.

*Corresponding author.
E-mail address:* mukherjee@ieee.org (B. Mukherjee).

## 1. Introduction

Interaction of high-energy particles with the structure of the accelerator facility results in the production of a parasitic radiation field composed of photo (fast) neutrons, muons and bremsstrahlung gamma-rays [1,2]. In high-energy electron linacs, photoneutrons are produced via three pathways [3]; (*a*) *Giant Dipole Resonance* (*GDR*) *reaction:* The impinging bremsstrahlung photons are absorbed in the target nuclei causing excitation. The photoneutrons are generated in de-excitation processes of the target nuclei. The angular distribution of the GDR-photoneutrons is isotropic and the production cross-section reaches its maximum at a photon energy interval of 10–30 MeV. (*b*) *Pseudo-deuteron formation*: Beyond the region of the GDR reaction, the high-energy photons (30 to ∼300 MeV) primarily interact with the neutron–proton pairs rather than with the whole target nuclei. The excited pseudo-deuterons finally break up producing high-energy neutrons. (*c*) *Photopion production*: Above the threshold of ∼140 MeV photoproduction of pions predominates. These photopions interact with the target material producing high-energy secondary neutrons.

Among the three photoneutron-production mechanisms, the cross-section of the low-energy GDR reaction is about one order of magnitude higher than that of the pseudo-deuteron and photopion production reactions, occurring at much higher photon energies. On the other hand, the photon intensity (fluence) of the high-energy tail of the photon (bremsstrahlung) spectrum is several orders of magnitude less than the intensity in the lower energy region (10–30 MeV), relevant to the GDR reaction. Therefore, the photoneutron yields (i.e. the photoneutron-production –cross-section weighted with the corresponding bremsstrahlung intensity) of pseudo-deuteron and photopion reactions are many orders of magnitude lower than that of the GDR-photoneutrons, and hence could be ignored [3]. On the other hand, the neutrons produced via the pseudo-deuteron and photopion reactions are highly penetrating, therefore contributing a significant dose outside the adequately shielded accelerator containment (vault), while the low-energy GDR neutrons are mostly attenuated

in the shielding wall [4]. A mixed-radiation field made of high-energy photons and GDR photoneutrons dominates the radiation environment in the linac tunnel. The energy spectrum of the GDR photoneutrons is similar to that of the fission spectrum and independent of the energy of the impinging electron beam [5,6]. This stray mixed neutron–gamma radiation field usually triggers the malfunction of the semiconductor based microelectronic and photonic devices situated in the vicinity of accelerator facility [7]. Hence, the characteristics of this radiation field must be well known in order to quantify the magnitude and time-scale of radiation effects in semiconductors [8] and subsequently be able to undertake suitable counter measures for their mitigation.

The above scenario motivated us to develop a reliable and user-friendly experimental technique for an explicit estimation of neutron and gamma doses inside the containment of high-energy electron accelerators.

The well-known TLD-700 ($^7$LiF: Ti, Mg) thermoluminescent dosimeter is sensitive to gamma-rays, as well as responsive to neutrons with energies above 100 keV [9]. On the other hand, the anion-deficient, carbon-doped aluminium oxide ($\alpha$-Al$_2$O$_3$: C) thermoluminescent dosimeter [10] commercially available as TLD-500 has a very low response to neutrons of all energies and heavy charged particles but possesses high sensitivity to gamma-rays [11,12]. These phenomena have been exploited for an accurate assessment of neutron and gamma doses originating from the mixed radiation field. The method is primarily based on thermoluminescence glow-curve (TLGC) analysis [13] of the TLD-700 and TLD-500 dosimeter pairs. This dosimetry technique was successfully implemented to evaluate the neutron and gamma doses inside the containment-tunnel of the 450 MeV electron linac operating in pulsed mode with a duty cycle of 10 Hz at the DESY Research Centre (Fig. 1).

## 2. Materials and methods

### 2.1. Selection criteria of the dosimeters

Albedo-type dosimeter made of TLD-600 ($^6$LiF: Mg, Ti) and TLD-700 ($^7$LiF: Mg, Ti)
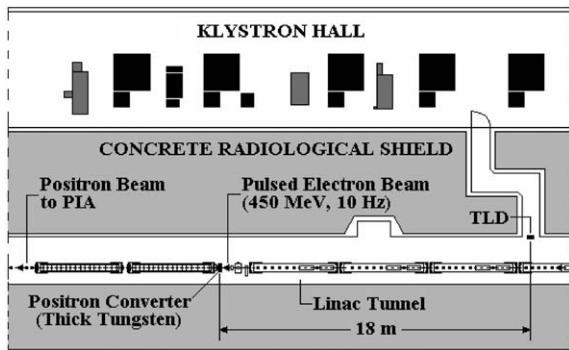
Fig. 1. Schematic diagram showing a part of the electron linac (DESY-Linac 2) tunnel highlighting the position of the thermoluminescent dosimeters (TLD) and tungsten positron converter bombarded with a 450 MeV pulsed electron beam producing intense fields of photoneutron and bremsstrahlung gamma-rays as parasitic radiations.

thermoluminescence dosimeters are now widely used in neutron–gamma personnel dosimetry [14]. A modified version of a similar dosimeter using TLD-600 and TLD-700 pairs has been used for the assessment of photoneutron and photon dose in a high-energy medical linac vault and reported elsewhere [15]. The main shortcoming of these types of dosimeter is the high thermal neutron sensitivity of TLD-600 ($^6$LiF: Mg, Ti), causing an over-response, even at very low thermal neutron fluence. This high thermal neutron sensitivity makes the TLD-600 and TLD-700 pair unsuitable for dosimetry of neutron–gamma mixed radiation fields [16,17]. We have circumvented the above pitfall by adopting the following measures and developed a fast-neutron/gamma dosimeter with negligible thermal neutron sensitivity.

Commercially available TLD-500 (dimension: 5 mm diameter × 1 mm, supplier: Studvik Instruments AB, Sweden) and TLD-700 (dimension: $3.2 \times 3.2 \times 0.9$ mm$^3$, supplier: Saint-Gobain Crystals, USA, formerly, Harshaw Chemicals Ltd.) were used in this project. The TLD-500 [12] and TLD-700 [13] chips were annealed separately, following proper procedures, and then individually enclosed in tiny photon energy compensating filters [18]. The TLD chips were divided into three equal batches each consisting of five pairs of TLD-500 and TLD-700.

## 2.2. TL dosimeter calibration

The dosimeters were calibrated for fast neutrons and gamma-rays using a 37 GBq $^{241}$Am–Be neutron-source (model: AMN 22 (X.3), manufacturer: Amersham International plc, UK) [19] and a 0.12 GBq (on 19 December 2003) $^{60}$Co gamma standard-source, respectively. The dose equivalent rates at 1 m from the $^{60}$Co and $^{241}$Am–Be sources ware supplied by the manufacturer as 40.5 μGy h$^{-1}$ and 27.3 μSv h$^{-1}$ ,respectively, and endorsed by the relevant statutory authority (TÜV Hamburg) as calibration benchmarks for the DESY radiation protection group. Prior to dosimeter irradiation, we checked the above benchmark dose rates using a gamma survey meter (model: Automess 6150AD6/E, manufacturer: Automation und Messtechnik GmBH, Germany) and an Anderson Braun-type neutron REM Counter (model: 2202 D, manufacturer: Studsvik Instrument AB, Sweden) issued with valid calibration certificates.

The dosimeter batches were exposed at 20 cm from the respective standard-sources. The inverse square law was applied to calculate the dose equivalent rates at dosimeter location and found to be 1012 μGy h$^{-1}$ and 684 μSv h$^{-1}$ for the gamma and neutron sources, respectively. The corresponding exposure time for gamma (142 mGy) and neutron (32.8 mSv) irradiation was calculated to be 140 h 29 min and 48 h, respectively. The dosimeter irradiation was performed in a dedicated experiment hall (4 m × 6 m) and the dosimeters were placed at 1.8 m from the floor level. The sufficiently large source-to-floor distance ensured a greatly reduced back-scattered radiation impinging on the dosimeters/ REM counter. In particular, this irradiation set up practically eliminated the influence of back-scattered slow (thermal) neutrons on the readout of the REM counter, which basically possesses a higher sensitivity to thermal neutrons.

It is evident that in addition to fast neutrons of an average energy of 4.2 MeV, a $^{241}$Am–Be (α, n)-neutron source also emits high (4.4 MeV)- and low (60 keV)-energy gamma-rays [20]. Our aim was to calibrate the TLD-500 and TLD-700

chips with a mixed gamma and neutron radiation field; hence, a bare [241]Am/Be neutron source was used without implementing any additional lead shielding.

## 2.3. Dosimeter irradiation at the 450 MeV electron linac

The third dosimeter batch was placed 1.2 m from the floor level near the entrance maze of the Linac 2 tunnel, at 18 m from the positron converter (Fig. 1).

The positron converter target (tungsten) was bombarded with a 450 MeV pulsed (10 Hz duty cycle) electron beam to produce positrons via the photonuclear reaction with tungsten atoms. The positrons were further accelerated, stored in the positron intensity accumulator (PIA) ring (not shown in Fig. 1) and finally injected to the DESY II booster synchrotron [21]. The positron converter target acts as the main source of the parasitic radiation, primarily composed of photo-neutrons and bremsstrahlung photons [3,5].

## 2.4. Readout procedure of the TL dosimeters

Twelve hours after irradiation in the electron linac tunnel, the TLD chips were sorted and stored in a light-tight box. All three batches of TLD chips were evaluated with an automatic TLD-Reader (model: TL 4500, manufacturer: Harshaw/Bicron Inc., USA). During readout, the TLD chips were heated from 50 °C (reader ambient temperature) to 350 °C at a ramp-heating rate of 10 °C s$^{-1}$ and the relevant TL-output data were stored in a personal computer. Each TLD chip was evaluated twice. The second reading was considered as the background data and subtracted from the first to obtain the net TL-output.

Prior to the operation of the TLD-Reader (TL-4500), its output range was set up by regulating the sensitivity of the photomultiplier-tube (PMT) used to detect the thermoluminescent glow. In this work we have adjusted the sensitivity of the PMT to obtain the following: 1 unit of PMT output (nC) = 1 unit of Reader output (arbitrary unit, a.u.).

The data files were finally assessed using a spreadsheet macro program for the purpose of TLGC analysis. The annealing, readout and data handling procedures of TLD-500 [12] and TLD-700 [13] have been described in detail elsewhere.

## 3. Results and data analysis

The Kinetic Energy Released in Materials (kerma) conversion factor (µGy/a.u.) of the [241]Am–Be neutrons for TLD-700 was evaluated from the experimental data, i.e. the TLGC-area and the neutron kerma coefficients of LiF adopted from Ref. [22]. Furthermore, by folding the neutron kerma coefficients [22] with the experimentally evaluated energy-spectra of the [241]Am–Be neutrons [23] and electron accelerator produced GDR photoneutrons [6], the kerma conversion factor for the latter was derived.

The TLGC of TLD-500 and TLD-700 pairs are interpreted as follows: The TLGC of TLD-500 chips irradiated with ^{60}Co-gamma-rays (Fig. 2a), [241]Am–Be neutrons (Fig. 2b) and photoneutron–gamma mixed radiation field in the Linac 2 tunnel (Fig. 2c) are shown as GC-a1, GC-b1 and GC-c1, respectively.

The TLGC of TLD-700 chips irradiated with ^{60}Co-gamma-rays (Fig. 2a), [241]Am–Be neutrons (Fig. 2b) and gamma/photoneutron mixed radiation field in the Linac 2 tunnel (Fig. 2c) are shown as GC-a2, GC-b2 and GC-c2, respectively. The maximum height of the high-temperature glow-peak (HTP) of TLD-700 irradiated with ^{60}Co gamma rays is indicated as $I_p$ (Fig. 2a). Furthermore, the TLGC area of TLD-500 and TLD-700 is represented as $A_{TLD500}$ (a.u.) and $A_{TLD700}$ (a.u.), respectively. Each TLGC shown in Figs. 2a–c represents the mean glow-curve derived from five individual TLD chips of the relevant batch. The TLGC evaluation results are summarised in Table 1.

The TLGC of TLD-700 is composed of several distinct glow-peaks, which occur within the temperature range 100 °C–350 °C [24]. In particular, the high temperature (∼310 °C) glow-peak (HTP) is primarily caused by densely ionising
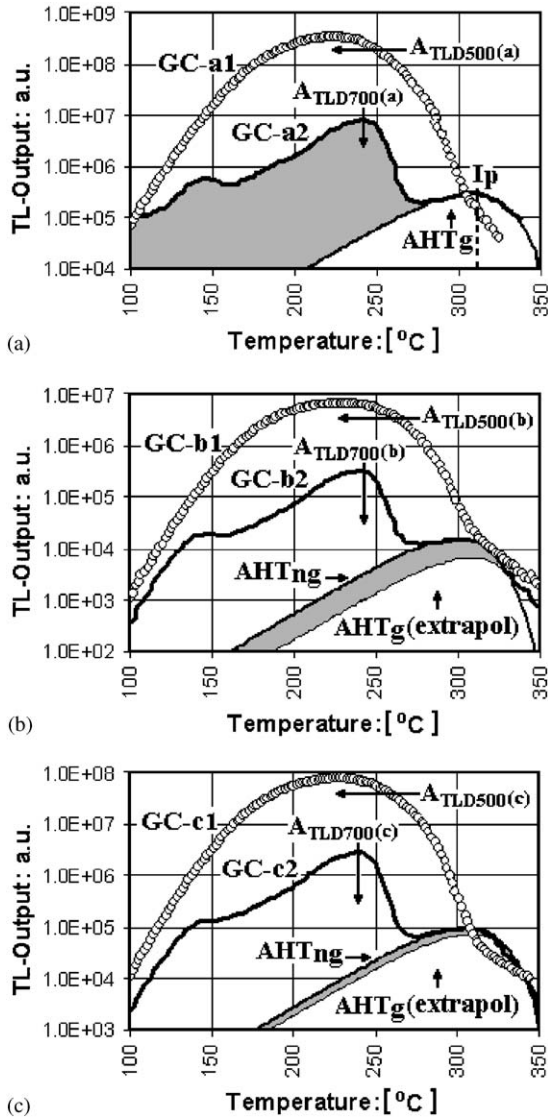
Fig. 2. The glow curves of TLD-500 and TLD-700 dosimeter pairs irradiated with (a) gamma-rays from a ^{60}Co source to 142 mGy, (b) fast neutrons from a [241]Am–Be source to 32.8 mSv and (c) gamma–photoneutron mixed radiation field produced by bombarding a thick tungsten positron converter target with a 450 MeV electron beam at Linac 2 (Fig. 1). The detail explanation of this figure is elucidated in Table 1 and in the main text.

(high LET) particles including fast neutrons. Furthermore, the HTP is also sensitive to gamma rays but to a lesser extent [13]. In the case of all

realistic radiation exposure scenarios, i.e. in a high-energy accelerator environment, the neutron field is always accompanied by gamma rays. Therefore, the gamma contribution of the high temperature glow-peak (HTP) must be well estimated prior to the application of the HTP area to evaluate the fast neutron kerma [13,16,17].

In order to assess the gamma background of the HTP, we developed a method based on the deconvolution of the TLGC of TLD-700 using the "Podgorsak" approximation of the 1st-order TL-kinetics model [13]. The application of the HTP deconvolution method for an explicit assessment of neutron and gamma doses in a mixed radiation field is described below.

### 3.1. Evaluation of the HTP-gamma background factor

The TLGC of TLD-500 (GC-a1) and TLD-700 (GC-a2) pair (Fig. 2a) were generated following an irradiation with gamma-rays from a 1.2 GBq ^{60}Co-source to 142 mGy. Obviously, the area under the deconvoluted HTP of TLD-700 ($AHT_g$) and the total TLGC-area ($A_{TLD500(a)}$) of the TLD-500 result from the same gamma exposure. Therefore, we defined a HTP-gamma background factor ($u_g$) for the TLD-700 in terms of TLGC-area of the TLD-500 as

$$u_g = AHT_g / A_{TLD500(a)} \tag{1a}$$

where $AHT_g$ ($1.01 \times 10^7$ a.u.) and $A_{TLD500(a)}$ ($1.29 \times 10^{10}$ a.u.) represent the HTP-area of TLD-700 and total TLGC-area of TLD-500 irradiated with ^{60}Co-gamma-rays (142 mGy), respectively. By substituting the numerical values (Table 1) in Eq. (1a) we obtain

$$u_g = 7.83 \times 10^{-4}. \tag{1b}$$

### 3.2. Evaluation of gamma dose calibration factor

The gamma dose component of the mixed neutron/gamma radiation was estimated using the area of the low-temperature part (marked as the grey area) of the TLGC of TLD-700 (Fig. 2a).

Table 1

Thermoluminescence glow-curve (TLGC) and glow-peak areas of the TLD-500 and TLD-700 pairs irradiated with gamma-rays ($^{60}$Co source), fast neutrons ($^{241}$Am–Be source) and neutron–gamma mixed radiation field produced at Linac 2 positron converter target. The TLGCs are shown in Fig. 2

| Type of dosimeter | TL-glow-curve and TL-glow-peak of interest | Glow-peak area (a.u.) | Type of radiation exposure |
|---|---|---|---|
| TLD−500 | GC-a1 (Fig. 2a) | — | D ($^{60}$Co-gamma)* |
| TLD-700 | GC-a2 (Fig. 2a) | — | D ($^{60}$Co-gamma)* |
| TLD-500 | $A_{TLD500(a)}$ (Fig. 2a) | $1.29 \times 10^{10}$ | D ($^{60}$Co-gamma)* |
| TLD-700 | $A_{TLD700(a)}$ (Fig. 2a) | $2.04 \times 10^{8}$ | D ($^{60}$Co-gamma)* |
| TLD-700 | $AHT_g$ (Fig. 2a) | $1.01 \times 10^{7}$ | D ($^{60}$Co-gamma)* |
| TLD-700 | $A_{TLD700(a)}$—$AHT_g$ (Fig. 2a) | $1.94 \times 10^{8}$ | D ($^{60}$Co-gamma)* |
| TLD−500 | GC-b1 (Fig. 2b) | — | H ($^{241}$Am–Be-neut)** |
| TLD-700 | GC-b2 (Fig. 2b) | — | H ($^{241}$Am–Be-neut)** |
| TLD-500 | $A_{TLD500(b)}$ (Fig. 2b) | $2.90 \times 10^{8}$ | H ($^{241}$Am–Be-neut)** |
| TLD-700 | $AHT_{ng}$ (Fig. 2b) | $5.22 \times 10^{5}$ | H ($^{241}$Am–Be-neut)** |
| TLD-700 | $A_{TLD700(b)}$ (Fig. 2b) | $8.41 \times 10^{6}$ | H ($^{241}$Am–Be-neut)** |
| TLD-700 | $AHT_g$(extrapol) (Fig. 2b) | $2.28 \times 10^{5}$ | H ($^{241}$Am–Be-neut)** |
| TLD-700 | $A_{TLD700(b)}$—$AHT_{ng}$ (Fig. 2b) | $7.89 \times 10^{6}$ | H ($^{241}$Am–Be-neut)** |
| TLD-700 | $AHT_{ng}$—$AHT_g$(extrapol) (Fig. 2b) | $2.95 \times 10^{5}$ | H ($^{241}$Am–Be-neut)** |
| TLD-500 | GC-c1 (Fig. 2c) | — | Linac 2 (mixed-field) |
| TLD-700 | GC-c2 (Fig. 2c) | — | Linac 2 (mixed-field) |
| TLD-500 | $A_{TLD500(c)}$ (Fig. 2c) | $3.18 \times 10^{9}$ | Linac 2 (mixed-field) |
| TLD-700 | $AHT_{ng}$ (Fig. 2c) | $3.33 \times 10^{6}$ | Linac 2 (mixed-field) |
| TLD-700 | $A_{TLD700(c)}$ (Fig. 2c) | $6.85 \times 10^{7}$ | Linac 2 (mixed-field) |
| TLD-700 | $AHT_g$(extrapol) (Fig. 2c) | $2.50 \times 10^{6}$ | Linac 2 (mixed-field) |
| TLD-700 | $A_{TLD700(c)}$—$AHT_{ng}$ (Fig. 2c) | $6.52 \times 10^{7}$ | Linac 2 (mixed-field) |
| TLD-700 | $AHT_{ng}$—$AHT_g$(extrapol) (Fig. 2c) | $8.28 \times 10^{5}$ | Linac 2 (mixed-field) |

* $D = 142 \, \text{mGy}$, ** $H = 32.8 \, \text{mSv}$.

The gamma dose calibration factor $\kappa_g$ is defined as:

$$\kappa_g = D_g/(A_{TLD700(a)} - AHT_g) \qquad (2a)$$

where $D_g$ (142 mGy), $A_{TLD700(a)}$ ($2.04 \times 10^8$ a.u.) and $AHT_g$ ($1.01 \times 10^7$ a.u.) represent the $^{60}$Co-gamma dose delivered to TLD-700, TLGC-area of TLD-700 and HTP-area of TLD-700, respectively. By substituting the numerical values (Table 1) in Eq. (2a) one obtains

$$\kappa_g = 7.32 \times 10^{-4} \, \text{mGy/a.u.} \qquad (2b)$$

### 3.3. Evaluation of neutron kerma in $^7LiF$

The TLGC of TLD-500 (GC-b1) and TLD-700 (GC-b2) pairs irradiated with neutrons from a 37 GBq $^{241}$Am–Be source [19] to 32.8 mSv are shown in Fig. 2b. The neutron fluence ($\varphi_{TLD}$) at

the location of TLD-500–TLD-700 pairs is calculated as follows:

$$\varphi_{TLD} = H/w \qquad (3a)$$

where $H$ (32.8 mSv) and $w$ ($3.91 \times 10^{-4} \, \mu\text{Sv cm}^2$) represent neutron dose equivalent delivered to the TLD chips and the neutron fluence to dose equivalent conversion factor according to the ISO standard [23], respectively. By substituting the numerical values in Eq. (3a) we obtain

$$\varphi_{TLD} = 8.39 \times 10^{7} \, \text{neutrons cm}^{-2}. \qquad (3b)$$

The neutron kerma of the $^{241}$Am/Be neutrons ($K_{AmLiF}$) delivered to $^7$LiF (the main component of TLD-700) is given as

$$K_{AmLiF} = \varphi_{TLD} \Sigma \Phi_{Am}(E) \times k_{LiF}(E) \qquad (4a)$$

where $\Phi_{Am}(E)$ and $k_{LiF}(E)$ represent the normalised energy spectrum of the $^{241}$Am/Be neutron

source [23] and neutron kerma factor distribution in $^7$LiF [22], respectively (Table 2). The neutron kerma delivered to TLD-700 with the same neutron fluence as from the $^{241}$Am–Be source ($\varphi_{TLD}$) but with an energy distribution of electron linac produced photoneutrons [6] $K_{PhLiF}$ is given as

$$K_{PhLiF} = f_c \times K_{AmLiF} \qquad (4b)$$

where $f_c$ represents the kerma conversion factor for photoneutrons, calculated by folding the neutron kerma distribution $k_{LiF}(E)$ in $^7$LiF with the normalised neutron spectra of the $^{241}$Am–Be source $\Phi_{Am}(E)$ and that of photoneutrons $\Phi_{Ph}(E)$:

$$f_c = \Sigma\Phi_{Ph}(E) \times k_{LiF}(E) / \Sigma\Phi_{Am}(E) \times k_{LiF}(E) \quad (4c)$$

By substituting the numerical values of $\varphi_{TLD}$ ($8.39 \times 10^7$ neutrons cm$^{-2}$) from Eq. (3b), $\Sigma\Phi_{Am}(E) \times k_{LiF}(E)$ ($8.84 \times 10^{-12}$ Gy cm$^2$) and $\Sigma\Phi_{Ph}(E) \times k_{LiF}(E)$ ($4.83 \times 10^{-12}$ Gy cm$^2$) from Table 2 we obtain

$$K_{AmLiF} = 7.42 \times 10^{-4} \, \text{Gy} \qquad (4d)$$

$$K_{PhLiF} = 4.05 \times 10^{-4} \, \text{Gy}. \qquad (4e)$$

### 3.4. Evaluation of neutron kerma calibration factor

The neutron kerma calibration factor for $^{241}$Am–Be neutrons ($\kappa_{AmLiF}$) and electron linac produced GDR photoneutrons ($\kappa_{PhLiF}$) in $^7$LiF are defined as follows:

$$\kappa_{AmLiF} = K_{AmLiF} / \text{AHT}_{net} \qquad (5a)$$

$$\kappa_{PhLiF} = K_{PhLiF} / \text{AHT}_{net} \qquad (5b)$$

where $\text{AHT}_{net}$ represents the net (gamma background subtracted) area under the deconvoluted HTP of TLD-700, which is exclusively linked to the neutron exposure.

A $^{241}$Am–Be neutron source also emits high-energy (4.4 MeV) gamma-rays [20] thereby contributing a significant level of gamma dose. This phenomenon was confirmed by TLGC area ($A_{TLD500(b)}$) of the neutron-insensitive TLD-500 (Fig. 2b).

The gamma background component ($\text{AHT}_{g(extrapol)}$) of the HTP of TLD-700 was

extrapolated using the gamma background factor $u_g$ (Eq. (1a)) and the corresponding TLGC-area of TLD-500:

$$\text{AHT}_g(\text{extrapol}) = u_g \times A_{TLD500(b)}. \qquad (5c)$$

By substituting the numerical values of $u_g$ ($7.83 \times 10^{-4}$) from Eq. (1a) and $A_{TLD500(b)}$ ($2.90 \times 10^8$ a.u.) from Table 1 in Eq. (5c) we obtain

$$\text{AHT}_g(\text{extrapol}) = 2.27 \times 10^5 \, \text{a.u.} \qquad (5d)$$

The net HTP area $\text{AHT}_{net}$, equivalent to neutron exposure (marked as the grey area in Fig. 2b) was calculated as

$$\text{AHT}_{net} = \text{AHT}_{ng} - \text{AHT}_{g(extrapol)} \qquad (5e)$$

where $\text{AHT}_{ng}$ represents the area under the HTP including the gamma background. By substituting the numerical values of $\text{AHT}_{g(extrapol)}$ ($2.27 \times 10^5$ a.u.) and $\text{AHT}_{ng}$ ($5.22 \times 10^5$ a.u.) from Table 1 in Eq. (5e) we obtain

$$\text{AHT}_{net} = 2.95 \times 10^5 \, \text{a.u.} \qquad (5f)$$

Furthermore, by substituting the numerical values of $K_{AmLiF}$ ($7.42 \times 10^{-4}$ Gy), $K_{PhLiF}$ ($4.05 \times 10^{-4}$ Gy) and $\text{AHT}_{net}$ ($2.95 \times 10^5$ a.u.) in Eqs. (5a) and (5b) the neutron kerma calibration factors for $^{241}$Am/Be neutrons and electron linac produced GDR photoneutrons are calculated as follows:

$$\kappa_{AmLiF} = 2.52 \times 10^{-3} \, \mu\text{Gy/a.u.} \qquad (5g)$$

$$\kappa_{PhLiF} = 1.37 \times 10^{-3} \, \mu\text{Gy/a.u.} \qquad (5h)$$

### 3.5. Dosimetry of neutron–gamma mixed radiation at electron linac

The neutron and gamma calibration factors evaluated from the deconvoluted TLGC of TLD-500 and TLD-700 dosimeters described in earlier sections were used to evaluate the neutron and gamma doses from the radiation field produced during the bombardment of a thick positron converter target (material: Tungsten) with a 450 MeV electron beam at an average current of 1.7 mA (Fig. 1). The TLGC of TLD-500 (GC-c1) and TLD-700 (GC-c2) irradiated with the mixed

Table 2
The kerma coefficient $k_{LiF}(E)$ of $^7$LiF [22] is shown as a function of neutron energy in the 2nd column. The normalised fluence of $^{241}$Am–Be neutrons and Giant Dipole Resonance (GDR) photoneutrons are shown in 3rd and 4th columns, respectively. The neutron kerma per unit fluence of the $^{241}$Am–Be and GDR photoneutron spectra are shown in 5th and 6th columns, respectively

| Group energy $E$ (MeV) | $\Phi_{Am}(E)$ (Normalised) | $\Phi_{Ph}(E)$ (Normalised) | $k_{LiF}(E)\ \Phi_{Am}(E)$ (Gy cm$^2$) | $k_{LiF}(E)\ \Phi_{Ph}(E)$ (Gy cm$^2$) |
|---|---|---|---|---|
| 4.14E−07 | 1.44E−02 | 9.33E−05 | 5.36E−15 | 3.47E−17 |
| 2.20E−01 | 3.34E−02 | 5.83E−02 | 2.81E−14 | 4.91E−14 |
| 4.35E−01 | 3.13E−02 | 7.04E−02 | 4.07E−14 | 9.15E−14 |
| 6.45E−01 | 2.81E−02 | 7.40E−02 | 4.90E−14 | 1.29E−13 |
| 8.60E−01 | 2.50E−02 | 7.34E−02 | 5.50E−14 | 1.61E−13 |
| 1.08E+00 | 2.14E−02 | 7.05E−02 | 5.67E−14 | 1.87E−13 |
| 1.29E+00 | 1.98E−02 | 6.64E−02 | 6.14E−14 | 2.06E−13 |
| 1.51E+00 | 1.75E−02 | 6.17E−02 | 6.22E−14 | 2.19E−13 |
| 1.72E+00 | 1.92E−02 | 5.68E−02 | 7.66E−14 | 2.26E−13 |
| 1.93E+00 | 2.23E−02 | 5.18E−02 | 9.89E−14 | 2.30E−13 |
| 2.15E+00 | 2.15E−02 | 4.69E−02 | 1.05E−13 | 2.29E−13 |
| 2.36E+00 | 2.25E−02 | 4.23E−02 | 1.20E−13 | 2.25E−13 |
| 2.58E+00 | 2.28E−02 | 3.80E−02 | 1.31E−13 | 2.19E−13 |
| 2.79E+00 | 2.95E−02 | 3.40E−02 | 1.83E−13 | 2.11E−13 |
| 3.01E+00 | 3.56E−02 | 3.03E−02 | 2.36E−13 | 2.01E−13 |
| 3.22E+00 | 3.69E−02 | 2.70E−02 | 2.61E−13 | 1.91E−13 |
| 3.43E+00 | 3.46E−02 | 2.40E−02 | 2.59E−13 | 1.80E−13 |
| 3.65E+00 | 3.07E−02 | 2.13E−02 | 2.43E−13 | 1.69E−13 |
| 3.86E+00 | 3.00E−02 | 1.88E−02 | 2.51E−13 | 1.57E−13 |
| 4.08E+00 | 2.69E−02 | 1.66E−02 | 2.36E−13 | 1.46E−13 |
| 4.29E+00 | 2.86E−02 | 1.47E−02 | 2.63E−13 | 1.35E−13 |
| 4.50E+00 | 3.18E−02 | 1.29E−02 | 3.06E−13 | 1.25E−13 |
| 4.72E+00 | 3.07E−02 | 1.14E−02 | 3.09E−13 | 1.14E−13 |
| 4.93E+00 | 3.33E−02 | 1.00E−02 | 3.49E−13 | 1.05E−13 |
| 5.15E+00 | 3.04E−02 | 8.78E−03 | 3.31E−13 | 9.57E−14 |
| 5.36E+00 | 2.74E−02 | 7.71E−03 | 3.10E−13 | 8.72E−14 |
| 5.58E+00 | 2.33E−02 | 6.75E−03 | 2.73E−13 | 7.93E−14 |
| 5.79E+00 | 2.06E−02 | 5.93E−03 | 2.50E−13 | 7.21E−14 |
| 6.00E+00 | 1.82E−02 | 5.19E−03 | 2.29E−13 | 6.52E−14 |
| 6.22E+00 | 1.77E−02 | 4.54E−03 | 2.30E−13 | 5.89E−14 |
| 6.43E+00 | 2.04E−02 | 3.97E−03 | 2.73E−13 | 5.32E−14 |
| 6.65E+00 | 1.83E−02 | 3.47E−03 | 2.52E−13 | 4.79E−14 |
| 6.86E+00 | 1.63E−02 | 3.04E−03 | 2.31E−13 | 4.31E−14 |
| 7.07E+00 | 1.68E−02 | 2.65E−03 | 2.45E−13 | 3.87E−14 |
| 7.29E+00 | 1.68E−02 | 2.32E−03 | 2.52E−13 | 3.47E−14 |
| 7.50E+00 | 1.88E−02 | 2.02E−03 | 2.90E−13 | 3.11E−14 |
| 7.72E+00 | 1.84E−02 | 1.76E−03 | 2.91E−13 | 2.78E−14 |
| 7.93E+00 | 1.69E−02 | 1.54E−03 | 2.74E−13 | 2.49E−14 |
| 8.14E+00 | 1.44E−02 | 1.34E−03 | 2.39E−13 | 2.22E−14 |
| 8.36E+00 | 9.68E−03 | 1.17E−03 | 1.64E−13 | 1.98E−14 |
| 8.57E+00 | 6.52E−03 | 1.02E−03 | 1.13E−13 | 1.77E−14 |
| 8.79E+00 | 4.26E−03 | 8.84E−04 | 7.57E−14 | 1.57E−14 |
| 9.00E+00 | 3.67E−03 | 7.69E−04 | 6.66E−14 | 1.40E−14 |
| 9.22E+00 | 3.81E−03 | 6.69E−04 | 7.07E−14 | 1.24E−14 |
| 9.43E+00 | 5.06E−03 | 5.84E−04 | 9.58E−14 | 1.10E−14 |
| 9.64E+00 | 6.25E−03 | 5.07E−04 | 1.21E−13 | 9.80E−15 |
| 9.86E+00 | 5.52E−03 | 4.41E−04 | 1.09E−13 | 8.68E−15 |
| 1.01E+01 | 4.68E−03 | 3.81E−04 | 9.40E−14 | 7.65E−15 |
| 1.03E+01 | 3.70E−03 | 3.29E−04 | 7.58E−14 | 6.75E−15 |
| 1.05E+01 | 2.78E−03 | 2.89E−04 | 5.79E−14 | 6.02E−15 |
| 1.07E+01 | 1.51E−03 | 2.53E−04 | 3.20E−14 | 5.37E−15 |
| 1.09E+01 | 3.63E−04 | 2.37E−04 | 7.75E−15 | 5.07E−15 |
|  | 1.00E+00 | 1.00E+00 | 8.84E−12 | 4.83E−12 |

photoneutron–bremsstrahlung radiations for 1 h are shown in Fig. 2c. All derived parameters, which include the TLGC area of TLD-500 ($A_{\text{TLD500(c)}}$) and TLD-700 ($A_{\text{TLD700(c)}}$), the area under the deconvoluted HTP ($\text{AHT}_{\text{ng}}$) and the extrapolated gamma background ($\text{AHT}_{\text{g(extrapol)}}$) are shown in Table 1. The gamma dose ($D_{\text{G}}$) and neutron kerma ($D_{\text{N}}$) were calculated as follows:

$$D_{\text{G}} = \kappa_{\text{g}} \times (A_{\text{TLD700(c)}} - \text{AHT}_{\text{ng}}) \tag{6a}$$

$$D_{\text{N}} = \kappa_{\text{PhLiF}} \times (\text{AHT}_{\text{ng}} - \text{AHT}_{\text{ng(extrapol)}}). \tag{6b}$$

By substituting the numerical values of $\kappa_{\text{g}}$ (7.32 $\times 10^{-4}\,\mu\text{Gy/a.u.}$), $\kappa_{\text{PhLiF}}$ (1.37 $\times 10^{-3}\,\mu\text{Gy/a.u.}$), $A_{\text{TLD700(c)}}$ ($6.85 \times 10^{7}\,\text{a.u.}$), $\text{AHT}_{\text{ng}}$ ($3.33 \times 10^{6}\,\text{a.u.}$) and $\text{AHT}_{\text{ng(extrapol)}}$ ($2.50 \times 10^{6}\,\text{a.u.}$) in Eqs. (6a) and (6b) we obtain

$D_{\text{G}}$ (gamma dose) $= 4.77 \times 10^{4}\,\mu\text{Gy}$

$D_{\text{N}}$ (neutron kerma) $= 1.14 \times 10^{3}\,\mu\text{Gy}.$

### 3.6. Discussion on sensitivity and dynamic range

The detection levels within a linear operating range of this neutron–gamma mixed radiation field dosimeter, including the gamma dose; GDR photoneutron kerma and fluence were exclusively determined by TLD-700. The TLD-500 was merely used to scale the gamma response of the HTP-area of the TLD-700, and hence had no direct influence in the sensitivity analysis.

The highest (HDL) and lowest (LDL) dose detection levels of the well-established TLD-700 are given as 1.0 Gy and 10 μGy, respectively [25]. Beyond an exposure level of 1.0 Gy the dose response of TLD-700 becomes "supra linear" and

the application of a complicated dose-correction factor becomes essential [25].

The highest detection level for photoneutrons kerma was estimated with the HTP area corresponding to the highest gamma dose, i.e. 1.0 Gy. The highest net-HTP area, assuming a 50% gamma contamination, was calculated to be $1.41 \times 10^{8}\,\text{a.u.}$, equivalent to a neutron kerma of $1.93 \times 10^{-1}\,\text{Gy}$. By applying the normalised fluence to kerma conversion factor (Table 2, Column 6) the maximum detectable neutron fluence was calculated to be $4.0 \times 10^{10}\,\text{cm}^{-2}$.

The lowest neutron kerma was evaluated from the lowest HTP-area deconvoluted using the lowest "detectable" HTP-intensity $I_{\text{p}}$ (Fig. 2a). The lowest $I_{\text{p}}$ was specified to be about four times of the background TL-signal at the HTP location, $\sim 310\,^{\circ}\text{C}$ (Fig. 2a). The mean background TL-signal was recorded by evaluating a set of five TLD-700 chips without radiation exposure and found to be 321 a.u., corresponding to an HTP-intensity (Ip) of 1284 a.u. The lowest detectable photoneutron kerma and fluence were calculated using the method described in an earlier paragraph and found to be $1.76 \times 10^{-6}\,\text{Gy}$ and $3.65 \times 10^{5}\,\text{cm}^{-2}$, respectively. The results including the dynamic ranges of the neutron–gamma mixed field dosimeter presented in this report are summarised in Table 3.

### 3.7. Discussion on errors and precautionary measures

The sensitivity of commercially available TLD chips often notoriously fluctuates. These large

Table 3
The dynamic range of the detection parameters of the neutron–gamma mixed radiation dosimeter presented in this report

| Detection levels | Gamma-rays | Photoneutron | Remarks |
|---|---|---|---|
| Highest detectable dose (Gy) | $1.0 \times 10^{0}$ | — | Ref. [25] |
| Lowest detectable dose (Gy) | $1.0 \times 10^{-5}$ | — | |
| Highest detectable kerma (Gy) | — | $1.93 \times 10^{-1}$ | This work |
| Lowest detectable kerma (Gy) | — | $1.76 \times 10^{-6}$ | |
| Highest detectable fluence (cm$^{-2}$) | — | $4.0 \times 10^{10}$ | This work |
| Lowest detectable fluence (cm$^{-2}$) | — | $3.65 \times 10^{5}$ | |

fluctuations obviously produce unacceptably high errors, which render the output-data into meaningless numbers. To avoid this drawback, we had irradiated 50 sets of TLD-500 and TLD-700 pairs with $^{60}$Co-gamma rays, evaluated individual TLD chips and selected 15 sets of TLD pairs with a batch inconsistency of less than $\pm 1\%$ for this experiment.

The selected TLD pairs were calibrated using a $^{60}$Co-gamma and a $^{241}$Am–Be neutron standard source kept at DESY radiation protection group. The gamma and neutron dose rates at 1 m from the standard sources were checked by a duly calibrated gamma radiation survey instrument and a neutron REM counter.

The gamma dose (142 mGy) and neutron dose equivalent (32.8 mSv) delivered to the TLD pairs during the calibration procedure were quite high, thereby causing a negligible systematic (calibration) error.

The Model 4500 TLD-Reader (manufactured by Harshaw/Bicron, USA) was used throughout the TL-readout process. The photomultiplier noise and light collection efficiency of the TLD-readout system were automatically examined; thereby delivering quality assured output data every time. All TLD phosphor, in particular the TLD-500 ($Al_2O_3$) is highly photosensitive [10], therefore, the TLD chips were handled in a climate-controlled room illuminated with a low-power incandescent lamp.

The TLGC-deconvolution of the HTP of TLD-700 using the "Podgorsak Approximation" of the 1st-order TL-kinetics model was optimised by the "least-squares fitting" technique aiming for the lowest root-mean-square (RMS) residue [13]. The large accumulated counts of the TLGC of TLD-500 and TLD-700 (Fig. 2a–c) caused a negligibly small random error. However, the errors of the RMS residue (deconvolution error) of the HTP of TLD-700 for all three TLGC (Fig. 2a–c) were much higher, i.e. $\pm 12\%$. The overall uncertainty of the gamma dose ($D_G$) and neutron kerma ($D_N$) estimated in the Linac environment was $\pm 15\%$ and $\pm 20\%$ respectively.

## 4. Summary and conclusion

This report highlights a novel dosimetry technique for the estimation of photoneutron and bremsstrahlung gamma dose contributions of the mixed radiation field produced by a 450 MeV electron linac operating at a pulse repetition rate (duty cycle) of 10 Hz.

The bremsstrahlung (gamma) dose and photoneutron kerma at 18 m from a thick tungsten target bombarded with a 450 MeV, 1.7 mA electron beam for 1 h were evaluated to be $4.77 \times 10^4$ and $1.14 \times 10^3 \, \mu Gy$, respectively.

The method is based on the estimation of the fast neutron kerma (dose) from the deconvoluted high-temperature glow peak (HTP) of the TLD-700 ($^7$LiF: Mg, Ti) dosimeter. The gamma background of the HTP was explicitly evaluated using the neutron insensitive TLD-500 ($\alpha$-$Al_2O_3$: C) dosimeter and subtracted from the total HTP-area to obtain the net neutron dose. Hence, the inconsistencies and shortcomings of HTP deconvolution technique for mixed radiation fields [17] were avoided.

Dosimeter pairs, consisting of TLD-500 and TLD-700 were initially calibrated using $^{60}$Co-gamma and $^{241}$Am–Be neutron standard sources. The neutron kerma calibration factor for the accelerator-produced GDR photoneutrons was evaluated by folding the respective neutron energy spectra with neutron kerma distribution in $^7$LiF (Fig. 3). The fluence to kerma conversion factor of photoneutrons for $^7$LiF (Columns 5, 6 of Table 2) is a pure "physical quantity" representing the energy transfer of unit neutron fluence to Lithium Fluoride. On the other hand, the fluence to dose equivalent conversion factor [26] proposed by the International Commission on Radiological Protection (ICRP) is an "operational quantity" valid for biological entities (soft tissue or tissue equivalent material). Hence, the two conversion factors shall not be compared with each other.

The unique characteristics of this neutron–gamma dosimeter include a large dynamic range, negligible thermal neutron sensitivity and a high gamma discrimination capability. Hence, this device has proved to be most suitable for dosimetry of fast neutrons superimposed with a
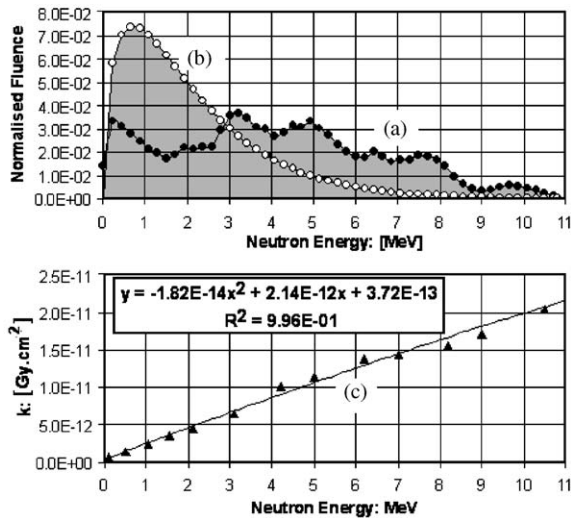
Fig. 3. The energy spectrum of the (a) $^{241}$Am–Be neutron source, (b) the GDR photoneutrons produced by a 450 MeV electron beam bombarding a thick tungsten target [6] and (c) the kerma coefficient ($k$) of $^7$LiF depicted as a function of neutron energy [22]. The areas under the spectra (shaded) are normalised to unity. The data-points are fitted with a 2nd-order polynomial shown inset.

strong gamma background. Furthermore, the possibility of a simultaneous evaluation of gamma dose and fast neutron kerma suggests the use of TLD-500 and TLD-700 pairs as a precursor of Total Ionising Dose (TID) and Single Event Upset (SEU) effects for the semiconductor circuitry [8] situated in the accelerator radiation environment. The repetition (pulse) rate of the radiation field has evidently no influence on the response characteristics of the TLD chips.

This makes the TLD-500 and TLD-700 pairs most suitable for the dosimetry of pulsed neutron-gamma radiation field produced by high-energy electron linacs, where conventional radiation detection instruments fail to operate optimally [27]. Obviously, the present device could also be used as a simple, inexpensive, general-purpose accelerator dosimeter for all major variants of high-energy electron accelerators, including, Booster-Synchrotron, Storage-Ring and Free Electron Laser.

## References

[1] J.C. Liu, J.S. Bull, J. Drozdoff, R. May, V. Vylet, Radiat. Prot. Dosim. 96 (2001) 429.
[2] W.P. Swanson, STI/DOC/10/188, International Atomic Energy Agency, Vienna, 1979.
[3] V. Vylet, J.C. Liu, Radiat. Prot. Dosim. 96 (2001) 333.
[4] V. Vylet, J.C. Liu, S.H. Rokni, L.X. Thai, Radiat. Prot. Dosim. 70 (1997) 425.
[5] X. Mao, K.R. Kase, W.R. Nelson, Health Phys. 70 (1996) 207.
[6] K. Tesch, Particle Accel. 9 (1979) 201.
[7] D. Makowski, B. Mukherjee, M. Grecki, S. Simrock, in: Proceedings of the XIV IEEE-SPIE Symposium on Photonics and Web Engineering, 26–30 May 2004, Wilga, Poland.
[8] M. Dentan, CERN Training Course, April 10–12, 2000, Geneva, Switzerland.
[9] S. Tanaka, Y. Furuta, Nucl. Instr. and Meth. 170 (1977) 395.
[10] M.A. Akselrod, V.S. Kortov, E.A. Gorelova, Radiat. Prot. Dosim. 47 (1993) 159.
[11] G.A. Klemic, N. Azziz, S.A. Marino, Radiat. Prot. Dosim. 65 (1996) 221.
[12] B. Mukherjee, A.C. Lucas, Radiat. Prot. Dosim. 47 (1993) 177.
[13] B. Mukherjee, Nucl. Instr. and Meth. A 385 (1997) 179.
[14] E. Piesch, B. Burgkhard, Radiat. Prot. Dosim. 23 (1988) 117.
[15] D.W. Anderson, C.C. Hwang, Health Phys. 44 (1983) 115.
[16] Y.S. Horowitz, S. Freeman, A. Dubi, Nucl. Instr. and Meth. 160 (1979) 317.
[17] Y.S. Horowitz, D. Satinger, E. Fuks, L. Oster, L. Podpalov, Radiat. Prot. Dosim. 106 (2003) 7.
[18] B. Burgkhardt, E. Piesch, H.G. Roeber, S. Ugi, Kerntechnik 55 (1990) 362.
[19] Neutron Sources Specification Sheet (Catalogue No. RS16-7), Amersham International, 1982, p. 5.
[20] H.R. Vega-Carrillo, E.A. Acuña, A.M. Becerra-Ferreiro, A. Carrillo-Nuñez, Radiat. Isot. 57 (2002) 167.
[21] H. Weise, DESY Machine Advisory Committee (MAC) Report, June 2003, Hamburg, Germany.

[22] R.S. Caswell, J.J. Coyne, M.L. Randolph, Int. J. Appl. Radiat. Isot. 333 (1982) 1227.

[23] Reference Neutron Radiations—Part 1: Characteristics and Methods of Production, ISO 8529-1, International Standard Organisation, 2001.

[24] D. Youssian, Y.S. Horowitz, Radiat. Prot. Dosim. 77 (1998) 151.

[25] S.W.S. McKeever, M. Moscovich, P.D. Townsend, Thermoluminescence Dosimetry Materials: Properties and Uses, Nuclear Technology Publishing, Ashford, Kent, UK, 1995.

[26] Conversion coefficients for use in radiological protection against external radiation, ICRP Publication 74, 1997.

[27] J.C. Liu, S. Rokni, V. Vylet, R. Arora, E. Semones, A. Justus, Radiat. Prot. Dosim. 716 (1997) 251.